Indian Journal of Pure & Applied Physics
Vol. 63, April 2025, pp. 281-300
DOI:10.56042/ijpap.v63i4.14388

Numerical Simulation on Sensitivity Modulation in Nanowire MOSFEB Detector for Biomedical Applications

Amit Das[a], Anjana Bhardwaj[a,*], Kaushik Das[b], Shivani Yadav[c], Aapurva Kaul[d], Preeti Goyal[e], Swati Sharma[e], Sonam Rewari[d], Binod Kumar Kanaujia[f] & R S Gupta[e]

[a]Department of Electronics and Communication Engineering, GLA University, Mathura, Uttar Pradesh 281 406, India

[b]Department of Electronics and Communication Engineering, National Institute of Technology Jamshedpur, Adityapur 831 014, India

[c]Department of Electronics and Communication Engineering, KIET Group of Institutions, Ghaziabad 201 206, India

[d]Department of Electronics and Communication Engineering, Delhi Technological University, New Delhi 110 042, India

[e]Department of Electronics and Communication Engineering, Maharaja Agrasen Institute of Technology, New Delhi 110 086, India

[f]Department of Electronics and Communication Engineering, Dr. B. R. Ambedkar National Institute of Technology Jalandhar 144 027, India

Received: 8 November 2024; accepted: 31 March 2025

The work aims to investigate and evaluate the biodetection capability of a nanowire MOSFEB detector for label-free biomedical applications. The study adopts a numerical computational-cum-simulation methodology to modulate, control and optimize sensitivity through dielectric modulation. Doping, a controllable factor prior to the fabrication process, plays a crucial role in enhancing the sensitivity of similar biosensors, thus making this work valuable. It is evident in the study that lower doping levels in the source and drain result in a greater percentage change in sensing metrics, whereas higher doping levels lead to a more significant relative change in sensing metrics. Additionally, the study comprehensively investigates the effect of drain voltage, material engineering, cavity dimensions/location, temperature, and device parameters on sensitivity. Sensitivity improvements of 18.573%, 13.979%, and 13.459% are achieved through gate, oxide, and channel engineering, respectively in the proposed biosensor. The study also addresses effect of trap charges on device reliability, alongside the calculation of the limit of detection. The results indicate that the silicon source exhibits better reliability and fewer short channel effects compared to other materials. Practical limiting factors have been taken into consideration in terms of non-unity fill-in factor and different filling profiles. The detector has also been compared with its junctionless variant, demonstrating a sensitivity enhancement of 95.716 mV for K_{bio}=5. The nanowire detector has been benchmarked against reported works in literature in terms of sensitivity.

Keywords: Biodetector, Cylindrical gate MOSFEB, Detector, FEB, MOSFEB, Nanosensor, Nanowire, Nanowire MOSFEB, NWM-BD, Subthreshold slope, SILVACO TCAD, Transistors

1 Introduction

Field effect transistors (FETs) have made substantial impact in the realm of electronics, offering a variety of specialized types that cater to a wide array of applications[1,2]. The versatility in FET is extensively utilized in the biomedical field, where it is used for different clinical tasks. One of the extensively researched applications is biosensing[3]. An exemplary biosensor should be highly sensitive to all the biomolecules, indicated by the difference in the value of different sensing metrics, demonstrating a high sensitiveness (response). The insertion of biomolecules into cavities primarily alters the profile of the channel's electric field and potential. Researchers have investigated different FET architectures for biomedical applications, such as extended-gate FETs, ion-sensitive FETs (ISFETs), and nanowire FETs, each offering specific benefits regarding sensitivity, selectivity, and fabrication simplicity[3-6]. The selection of semiconductor materials is also significant; silicon is widely used due to its simplified (common) processing methods, while new materials like graphene and molybdenum disulfide are promising for improved analog performance.

A biosensor is an analytical device used for the rapid detection of bio-chemical species (biomolecules). Biosensors are either label-based, using unique labels to identify targets, or label-free, suitable for untagged

*Corresponding author: (E-mail: anjana.0889@gmail.com)

analytes. The choice between these approaches is contingent upon the specific analytical requirements and the biochemical properties of the target analytes[7]. Label-free detectors offer particular utility in scenarios where molecular tagging is challenging or undesirable, and for the direct detection of unmodified target entities (biochemical species). Conversely, label-based detectors leverage the unique properties of molecular tags to achieve highly specific target identification (improving specificity). Label-less detection is preferred for its simplicity, affordability, and suitability for real-time analysis. Due to their exceptional sensitivity, MOSFET based label-free biosensors (MOSFEB)[4] have garnered significant popularity in the field of bioelectronics[8]. Harnessing the remarkable properties of semiconductors, MOSFEB stands at the forefront of biotechnology, along with its integration with nanotechnology innovation. By capitalizing on the subtle modulation of electrical properties upon biomolecular interactions, these biosensors enable label-free, rapid, and ultrasensitive detection, underscoring their role in revolutionizing fields such as personalized medicine and bioprocess monitoring[9]. These biosensors use the molecular properties (dielectric constant and charge density) of different biochemical species for label-free detection, which means that the device can directly detect the test biomolecule without any tagged entity[4]. The primary principle behind the detection ability of every MOSFEB is dielectric modulation of the sensing parameter. Figure 1 (a-b) demonstrate the fundamental device principle and basic detection principle in nanowire MOSFEB. These detectors leverage selective biorecognition elements to detect and quantify target analytes such as biomolecules, pathogens, or chemicals. The threshold voltage is the commonly used sensing parameter, but apart from this, various characteristics like subthreshold slope, off-current, I_{ON}/I_{OFF} ratio, and transconductance can be used to analyze the sensitivity. The detector derives its name from the fact that it uses a transistor whose charge carrier transportation mechanism is modulated by electric field (FET), and it incorporates dielectric engineering (MOS) for label-free detection of biochemical species. Hence, the name Nanowire MOSFEB Detector (Nanowire MOSFET + Biomolecules Detector: MOSFET for biomolecules detection), abbreviated as NWM-BD. The term "nanowire" in nanowire MOSFEB refers to its surrounding gate (SG) architecture, which enhances electrostatic control over the channel and improves charge carrier transport. The versatility of MOSFEB extends beyond their basic operational principle, encompassing a wide array of design variations and sensing mechanisms.

Several researchers have explored the concept of biomolecule sensing in transistors through gate oxide modulation. But not much-related work (doping dependent sensitivity analysis) has been done in the past, a very few authors have partially shown the effect of doping on sensitivity[10,11]. The effect of channel doping on the sensitivity of a junctionless biosensor was recently discussed[8]. Recently, a few authors have reported nanotube FET-based biosensors for detecting the biomolecule species using different sensing metrics[4,12]. Authors, such as Yadav *et al.*[13], Sharma *et al.*[9], Kumari *et al.*[14], Goel *et al.*[15] and many more, have recently reported different types of FET-

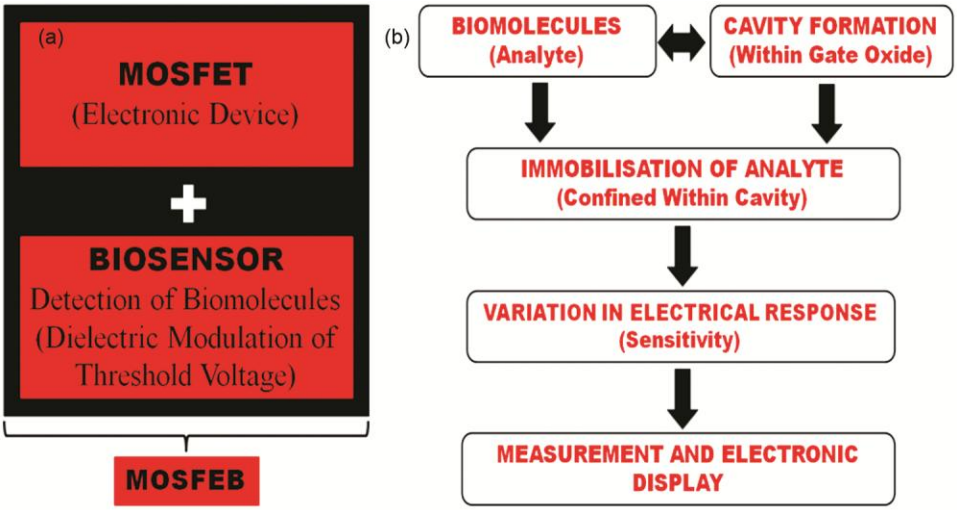

Fig. 1 — (a) Device principle, and (b) flowchart of the generalized biosensing phenomenon in NWM-BD[8,9]

based biosensors based on dielectric engineering. Upon reviewing various literature sources, it becomes apparent that researchers have investigated various potential variants for BioFETs. However, detailed exploration of doping-dependent sensitivity modulation remains largely unexplored in the existing research. Hence, the novelty of this paper as well as main goal of this work is to examine the sensitivity modulation in the nanowire MOSFEB because of doping. Doping becomes critically important in controlling and modulating sensitivity, as it is a parameter that can be adjusted before fabrication[16], highlighting the significance of this research. The second objective is to explore the other side of the nanowire MOSFEB detector, which includes studying the effect of temperature, structural parameters, trap charges, drain bias, source/channel/drain engineering techniques as well as steric hindrance on the sensitivity.

2 Device Structure and Computational Framework

2.1 MOSFEB Specifications

3D and 2D view of the nanowire MOSFEB detector is shown in Fig. 2 (a-b), respectively. The proposed detector, employing dielectric engineering by immobilizing biomolecules within the embedded cavity, is specifically designed for detecting various charged and neutral biochemical species. The measurable response of the detector is defined by changes in threshold voltage or subthreshold slope, although several other metrics have also been taken into consideration. A poly-silicon gate (work function: 4.96 eV) has been used, which has the advantage regarding fabrication simplicity and increased operating temperature range over the metallic gate. A symmetric and two-sided cavity of dimensions 14*2 nm^2 is embedded inside SiO_2 layer[8,12]. Figure 2(c) shows the detailed fabrication steps[17-19]of the proposed biosensor in the form of a flowchart. A precise cavity with the specified dimensions can be created using multiple rounds of dry etching, without compromising the quality of the gate oxide[20]. The biosensor features a dual cavity of 14×2 nm², enabling immobilization of biomolecules smaller than 14 nm, with the maximum detectable size depending on orientation (up to 14 nm horizontally and 2 nm vertically). This study primarily focuses on the upper detection limit, assuming full cavity occupancy while accounting for steric hindrance effects.

2.2 Simulator Setup and Specifications

The proposed biosensor's behavior is examined using parameters specified in Table 1 through the SILVACO TCAD simulator[21]. Various models are integrated into the simulation: the SRH model manages carrier generation and recombination, the CONMOB model correlates impurity profiles with low-field mobility at room temperature, and the AUGER model accommodates recombination effects at high doping densities. Additionally, the CVT model encompasses dependencies of mobility on doping, temperature, and field, while the FLDMOB model addresses field-dependent mobility. The BGN model handles bandgap narrowing attributed to degenerate as wellas high doping levels, and NEWTON

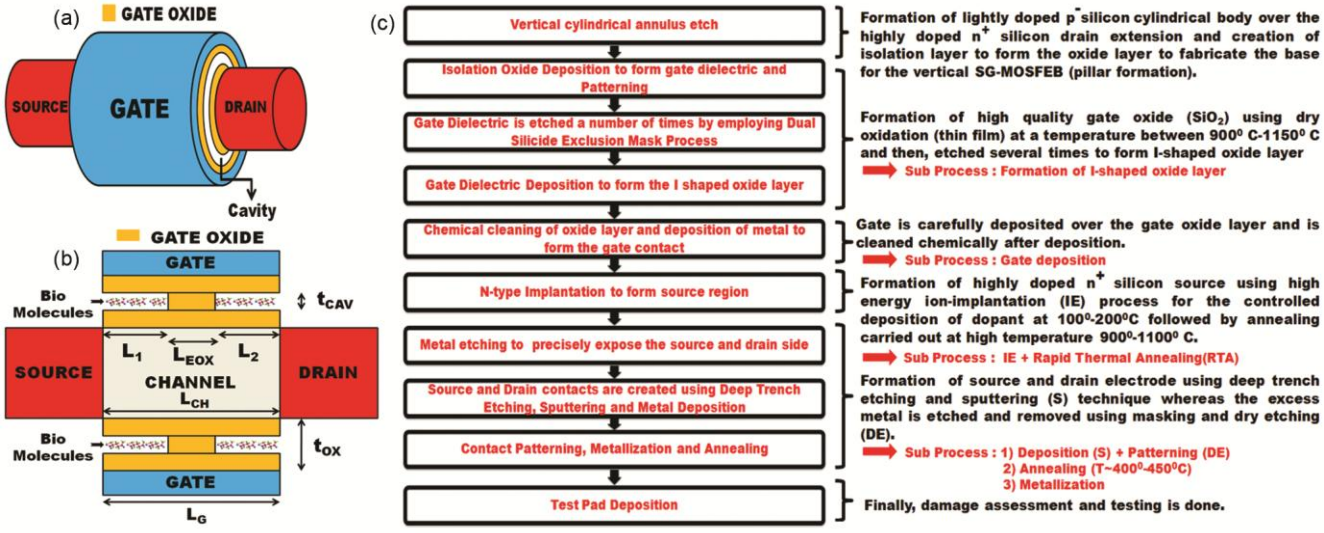

Fig. 2 — (a) 3D view, (b) 2D view, and (c) fabrication process flow-chart illustrating the basic fabrication steps of NWM-BD[20]

GUMMEL method is implemented to resolve the intricate, nonlinear coupled equations.

2.3 Methodology

Charge density (ρ) as well as dielectric constant (K_{bio}) is used to characterize various biomolecules. Biomolecules are either neutral (ρ=0) or charged (ρ≠0) with some finite dielectric constant. The different test biomolecules used in this study are mentioned in Table 1. Here, ρ of the biomolecule is kept constant, while keeping constant K_{bio}=5 to cover a large number of biomolecules (positively/neutral/negatively charged biomolecules). It is assumed that the cavity is occupied by air (dielectric constant of air is taken as K_{air}=1) in the absence of biomolecules[9,12]. When the test biomolecule (K_{bio}≠1) gets immobilized inside the cavity, threshold voltage (along with other device characteristics) gets changed because lateral field and gate oxide capacitance undergo changes when biomolecules are localized inside the cavity. Thus, the potential distribution gets modified across the channel[8, 24]. The relative difference in the sensing parameter's value is used as the qualitative indicator in the biosensing investigation of a nanowire MOSFEB detector. The numerical computational methodology used for the sensitivity analysis is shown in Fig. 3 as a flowchart. The relative change in the sensing metric (first formula) is preferred over fractional or percentage change for evaluating the biosensing performance. It provides a more accurate measure of sensitivity by directly comparing baseline and sensing values, whereas fractional or percentage change is tied to relative values, which may misrepresent true sensitivity.

Table 1 — Structural parameters of NWM-BD

Parameters		Value
Cavity thickness (t_{cav})		2-8 nm
Gate length (L_G)		30 nm
Source doping (N_S)		$1*10^{13}$ to $5*10^{20}$/cm^3
Channel length (L_{CH})		30 nm
Material	Source	n-type
	Channel	p-type Silicon
	Drain	n-type
Channel doping (N_C)		10^{10}/cm^3
Drain doping (N_D)		$1*10^{13}$ to $5*10^{20}$/cm^3
Drain/Source length		10 nm
Total oxide layer thickness (t_{ox})		4-10 nm
Biasing		V_{DS}=(0-1) V V_{GS}=(0-1) V
Drain/Channel/Source radius		10 nm
Cavity length		L_1= 14nm L_2= 14nm
Gate oxide		SiO_2
Gate work-function		4.96 eV
Oxide length (L_{OX})		L_{OX}= 30nm
BIOMOLECULES		
Hydroprotein(K_{bio}=5)[15]		
DNA (K_{bio}=5 & ρ= -1*10^{11}/cm^2)[22]		
Amino acids (K_{bio}=5 & ρ= +1*10^{11}/cm^2)[23]		

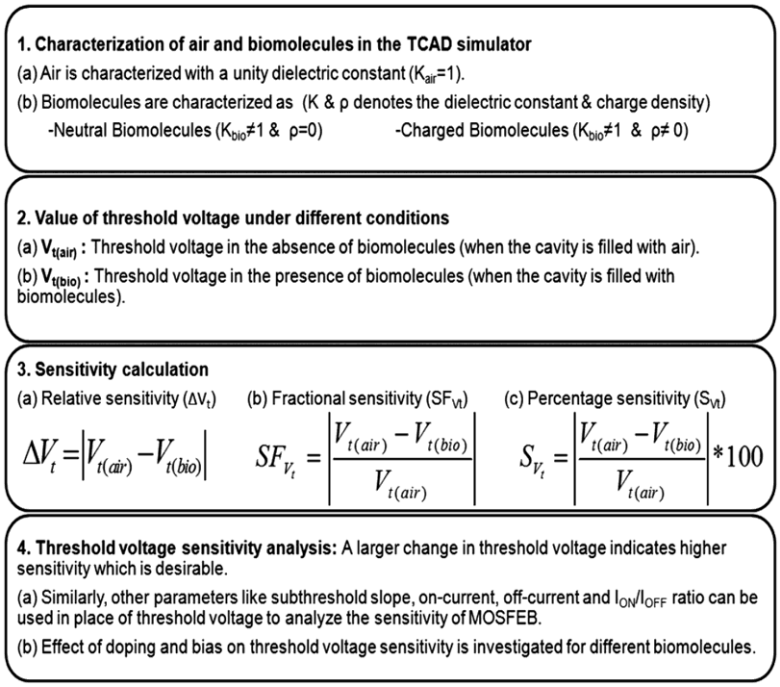

Fig. 3 — Computational methodology flowchart for sensitivity analysis

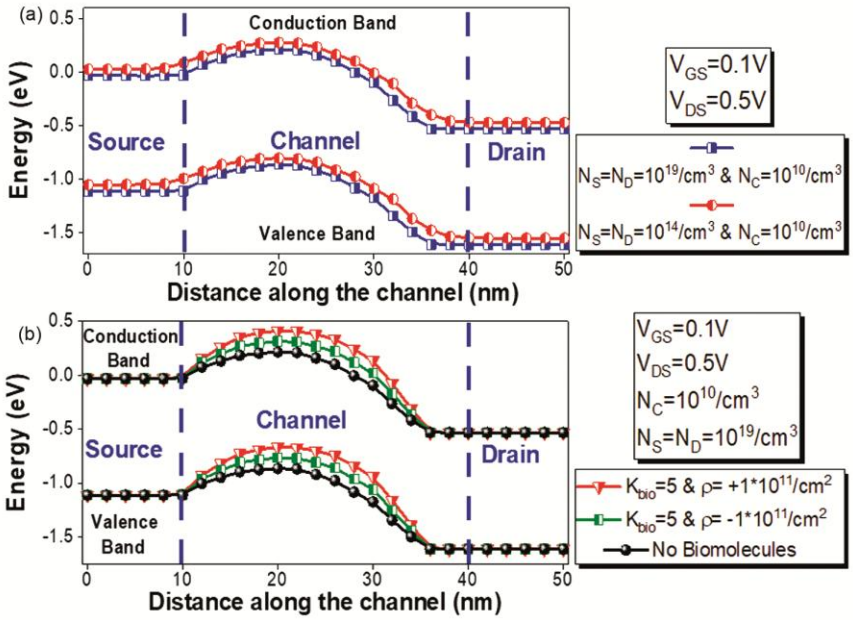

Fig. 4 — (a) Energy band diagram at various drain/source doping in the absence, and (b) presence of biomolecules in NWM-BD

3 Results and Discussion

3.1 Energy Band Diagram and Potential

Figure 4 illustrates the shift across energy bands within the nanowire MOSFEB detector across various operational conditions. In Fig. 4 (a), changes in drain/source doping levels lead to shifts in energy band positions; higher doping levels in the source increase electron density, pulling the bands downwards (Fermi level tends to moves inside the conduction band in n-type drain/source). Meanwhile, Fig. 4 (b) demonstrates how different biomolecules inside the cavity affect the positions of energy bands, influencing both the lateral electric field and gate capacitance in the channel. This interaction results in slight adjustments to the energies of both valence band as well as conduction band[8]. Contour plots in Fig. 5(a-c) depicts electron concentration profiles for negatively, neutral, and positively charged bio-chemical species.

Figure 6 presents the electron concentration contour plot across the channel in the nanowire MOSFEB detector, depicting different doping conditions. In Fig. 6(a), the contour plot shows the density of electrons at $N_C=10^{10}/cm^3$ and $N_D=N_S=10^{14}/cm^3$. In contrast, Fig. 6(b) shows the electron concentration contour plot at $N_S=N_D=10^{19}/cm^3$ and $N_C=10^{10}/cm^3$. It is evident that the peak electron concentration is localized near the channel surface. The localization of peak electron concentration near the channel surface underscores

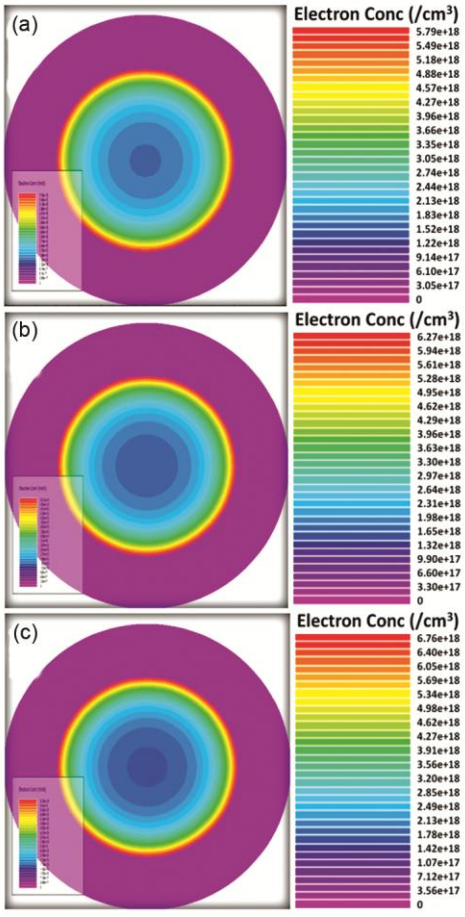

Fig. 5 — Contour plot of density of electrons (K_{bio}=5, $N_C=10^{10}/cm^3$,$N_D=N_S=10^{19}/cm^3$& $V_{DS}=V_{GS}$=1V) at different charge density (a) ρ=-1*10^11/cm^2, (b) ρ=0, and (c) ρ=+1*10^11/cm^2 of biomolecules in NWM-BD

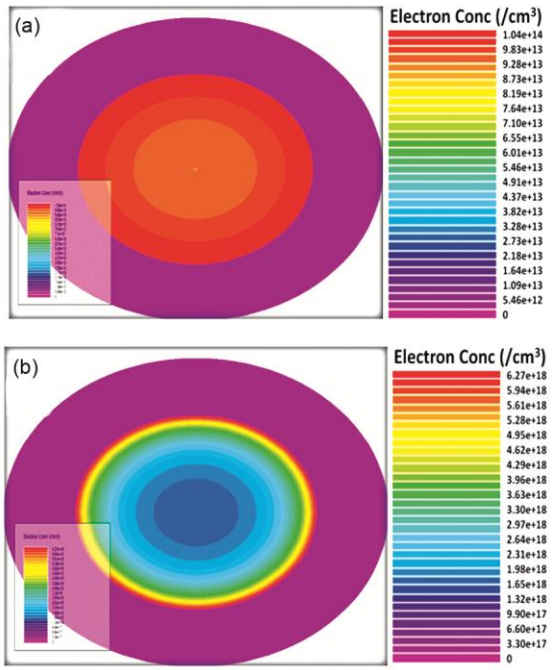

Fig. 6 — Contour plot of density of electrons (K_{bio}=5 & V_{GS}=V_{DS}=1V) at (a) N_C=10^{10}/cm^3, N_S=N_D=10^{14}/cm^3, and (b) N_C=10^{10}/cm^3, N_D=N_S=10^{19}/cm^3 in NWM-BD

the importance of surface phenomena in MOSFEB. Increasing the source doping enhances the electron concentration, thereby influencing the drain current[25]. The presence of bio-chemical species changes the electron concentration near the Si-SiO_2 interface by increasing the gate capacitance. The influence of biochemical species on the gate capacitance, as evidenced by the electron concentration changes, underscores the device's capability for label-free detection[8,26,27].

Figure 7 of the nanowire MOSFEB detector, the potential profile across the channel is illustrated. The main plot illustrates variations in the potential profile due to different doping levels of the source and drain. Meanwhile, the inset focuses on the potential profile in the presence of different biomolecules. Modifying the doping levels of the drain and source adjusts the potential barriers at the drain-channel and source-channel junctions, influencing the overall potential distribution across the channel[25,28]. The presence of biomolecules changes the gate capacitance and field profile, which in turn modifies the channel potential. Increasing the doping levels of the drain and source results in a notable rise in the channel's potential.

3.2 Effect of Equal Drain and Source Doping

Increasing the doping levels of both the source and drain results in two primary effects[16,29]. As the doping

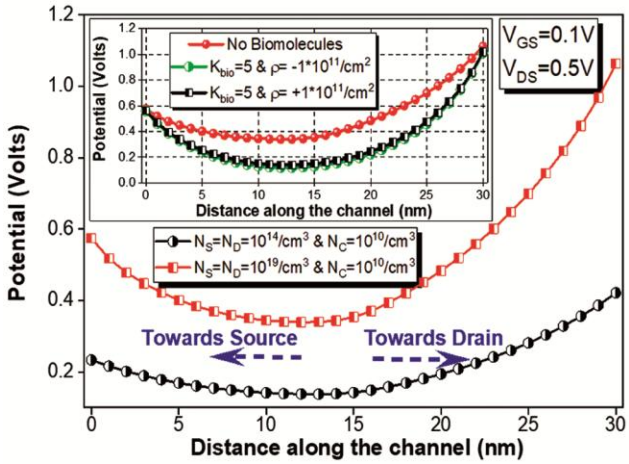

Fig. 7 — Potential profile across the channel at different source/drain doping in NWM-BD(*[INSET] Shows the potential profile across the channel in the presence of different biomolecules*)

levels of the drain and source are raised uniformly from low to high values, 'Effect 1' is observed, where a significant portion of the depletion region extends into the channel. 'Effect 2', on the other hand, involves a gradual reduction in the overall width of the depletion layer with increasing doping. Thus, both 'Effect 1' and 'Effect 2' become evident as the doping level of the drain and source increases. 'Effect 2' predominates at lower doping levels, reducing the depletion layer width and effectively increasing the channel length. Conversely, at higher doping levels, 'Effect 1' becomes more prominent, causing the depletion region to penetrate deeper into the channel and thereby decreasing the effective channel length. Figure 8 visually illustrates both 'Effect 2' and 'Effect 1'. The notation a_b_c denotes the doping levels of the source ($1*10^a$ cm^{-3}), channel ($1*10^b$ cm^{-3}), and drain ($1*10^c$ cm^{-3}), respectively, while S_C_D refers to source_channel_drain.

Table 2 presents data on the threshold voltage and its corresponding sensitivity across various doping levels (with same drain and source doping), considering different biomolecules filling the cavity. Initially, as doping increases, 'Effect 2' predominates by narrowing the depletion width. This reduces the depletion region coverage at the channel ends, thereby increasing the effective channel length. Consequently, a higher gate voltage is required to activate the device, resulting in an increase in the threshold voltage. As doping levels further increase, 'Effect 1' becomes more dominant. With higher source and drain doping compared to the channel, the depletion region extends significantly into the channel at both

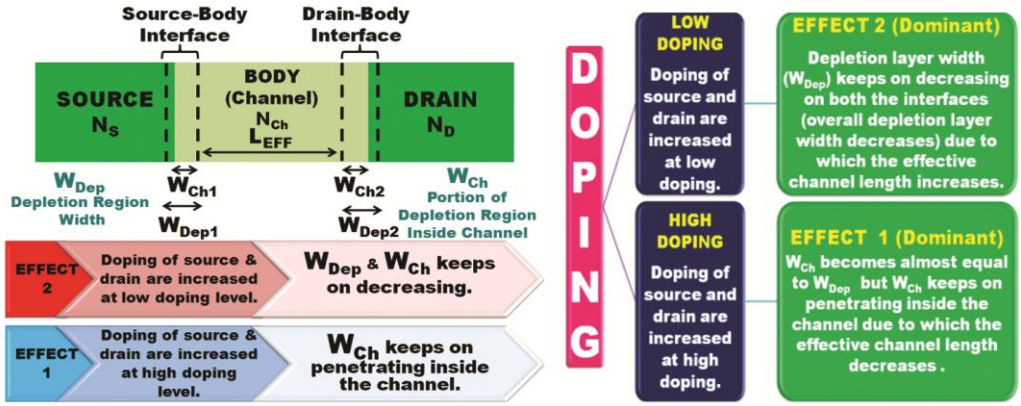

Fig. 8 — Visualization of the effect of doping on effective channel length in MOSFEB

Table 2 — Threshold voltage and threshold voltage sensitivity at different doping

	Doping (cm^{-3}) Source_Channel_Drain	Threshold Voltage (V_t : Volt)			Threshold Voltage Sensitivity (S_{Vt} : Percentage)		
		k_{bio} = 5					
		ρ $-1*10^{11}$ cm^{-2}	ρ 0	P $+1*10^{11}$ cm^{-2}	ρ $-1*10^{11}$ cm^{-2}	ρ 0	P $+1*10^{11}$ cm^{-2}
D_a	10^{13}_10^{10}_10^{13}	0.0459207	0.045366	0.0429468	453.0462	446.3645	417.2300
D_b	10^{14}_10^{10}_10^{14}	0.141106	0.134749	0.121702	264.6235	248.1967	214.4828
D_c	10^{15}_10^{10}_10^{15}	0.208939	0.202324	0.200550	65.7943	60.5452	59.1376
D_d	10^{16}_10^{10}_10^{16}	0.244491	0.241664	0.236106	49.4078	47.6803	44.2838
D_e	10^{17}_10^{10}_10^{17}	0.330133	0.315766	0.286625	44.9446	38.6368	25.8424
D_f	10^{18}_10^{10}_10^{18}	0.388328	0.371414	0.349767	40.7057	34.5771	26.7336
D_g	10^{19}_10^{10}_10^{19}	0.430309	0.416805	0.402911	74.1571	68.6916	63.0684
D_h	10^{20}_10^{10}_10^{20}	0.411948	0.399756	0.387387	133.8607	126.9394	119.9176

junctions. This shortens the effective channel length, requiring less gate voltage to activate the device and causing a reduction in the threshold voltage[16].Hence, the threshold voltage initially rises with doping, reaching a maximum value, but beyond a certain doping level, it begins to decrease, as depicted in Fig. 9(a). As seen in Fig. 9(b), although the sensitivity obtained is quite high at low doping, the conductivity of the device is quite low at such low doping, which limits the selection of low doping for MOSFET. The doping values D_a-D_h are specified in Table 2. In the current study, the threshold voltage sensitivity modulus is considered and given in Eq. 1. Since sensitivity is measured in terms of magnitude (i.e., the change in the sensing metric) rather than the sign of this change, taking the modulus ensures a consistent and comparative assessment of biosensor performance across different operational conditions.

$$S_{V_t} = \left| \left(\frac{V_{t(air)} - V_{t(bio)}}{V_{t(air)}} \right) * 100 \right| \quad \ldots (1)$$

At lower doping levels, 'Effect 2' tends to be predominant[30]. Increasing the doping of both the source and drain reduces the depletion width at the junctions of the drain-channel and source-channel, resulting in an increase in the depletion capacitance (C_{dep}). The subthreshold swing, inversely related to the subthreshold slope and directly proportional to C_{dep}, consequently increases as the depletion width decreases. This leads to a decrease in the subthreshold slope at lower doping levels[29,31]. At higher doping levels, 'Effect 1' becomes dominant, causing an increase in the subthreshold slope. A local minimum in the subthreshold slope can be seen in Fig. 10.

Table 3 illustrates the subthreshold slope observed at various symmetric doping levels for the source and drain. This metric is influenced by the doping levels of the drain, channel, and source, as well as by the presence of biomolecules within the cavity. Initially, the subthreshold slope sensitivity (S_{SS}) decreases until it reaches a minimum value, reflecting the relative difference $|SS_{(air)} - SS_{(bio)}|$ (where $SS_{(air)}$ and $SS_{(bio)}$

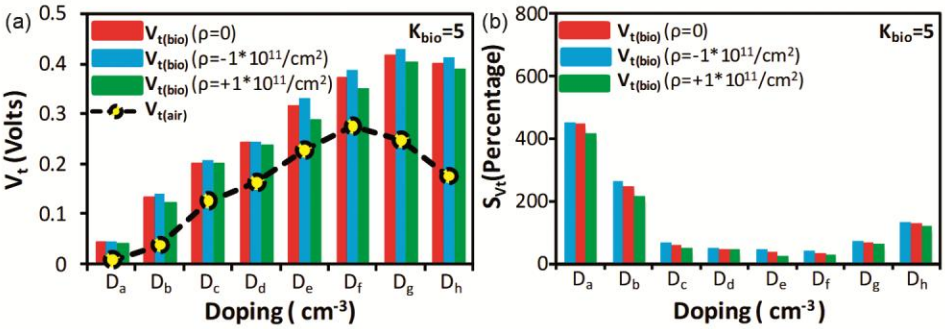

Fig. 9 — (a) V_t, and (b) S_{Vt} at different doping (N_C=10^{10}/cm^3, V_{DS}=0.5V & K_{bio}=5) in NWM-BD

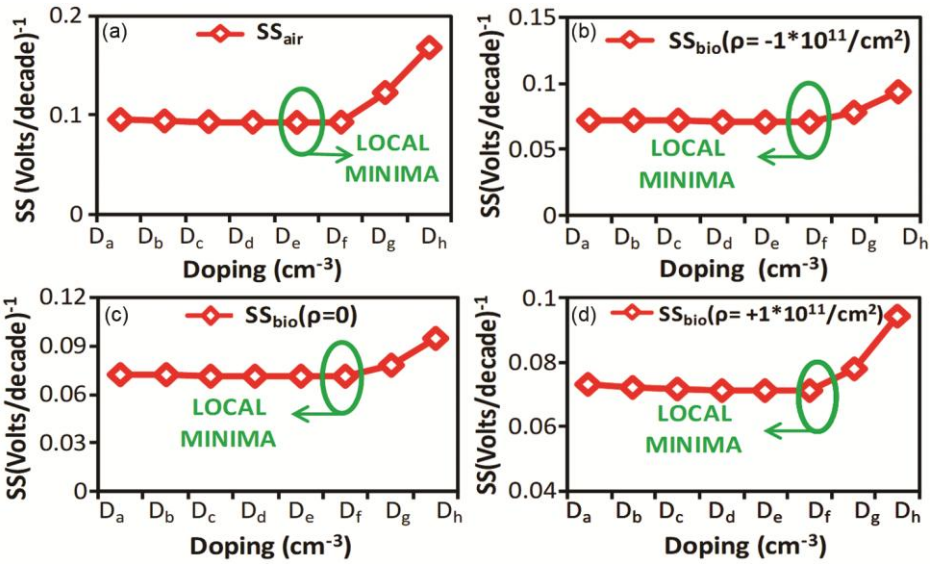

Fig. 10 — SS variation in the NWM-BD for (a) air, (b) negatively charged (ρ=-1*10^{11}/cm^2), (c) neutral (ρ=0), and (d) positively charged (ρ= +1*10^{11}/cm^2) biomolecules at different doping (K_{bio}=5, V_{DS}=0.5V, K_{bio}=5 & N_C=10^{10}/cm^3)

Table 3 — Subthreshold slope and subthreshold slope sensitivity at different doping

	Doping (cm^{-3}) S_C_D	Subthreshold Slope (SS : (Volts/decade)$^{-1}$)			Subthreshold Slope Sensitivity (S_{SS} : Percentage)		
		k_{bio} = 5					
		ρ -1*10^{11} cm^{-2}	ρ 0	P +1*10^{11} cm^{-2}	ρ -1*10^{11} cm^{-2}	ρ 0	P +1*10^{11} cm^{-2}
D_a	10^{13}_10^{10}_10^{13}	0.07194	0.0720	0.0729	25.1176	25.0421	24.0700
D_b	10^{14}_10^{10}_10^{14}	0.07193	0.07196	0.07196	24.0830	24.0579	24.0545
D_c	10^{15}_10^{10}_10^{15}	0.07148	0.07142	0.07141	23.9825	24.0456	24.0495
D_d	10^{16}_10^{10}_10^{16}	0.07128	0.07128	0.07128	23.8258	23.8267	23.8257
D_e	10^{17}_10^{10}_10^{17}	0.07121	0.07121	0.07121	23.6722	23.6692	23.6660
D_f	10^{18}_10^{10}_10^{18}	0.07114	0.07115	0.07115	23.9660	23.9640	23.9606
D_g	10^{19}_10^{10}_10^{19}	0.07747	0.07761	0.07776	37.1150	36.9970	36.8762
D_h	10^{20}_10^{10}_10^{20}	0.09395	0.09407	0.09423	44.1769	44.1020	44.0106

indicate the subthreshold slope with the cavity filled with air and biomolecules, respectively). Further equal increase in the doping rate leads to an enhancement in the S_{SS}. This trend is depicted in Fig. 11(a), 11(b), and 11(c), which shows the S_{SS} with negatively charged, neutral, and positively charged biomolecules in the cavity, respectively. The presence of charged biomolecules alters the flat-band voltage, thereby modifying the channel's field and potential profile[8, 15]. Table 3 also provides details on the

subthreshold slope sensitivity at different doping levels when the cavity immobilizes various biomolecules. Equation (2) outlines the formula for subthreshold slope sensitivity, emphasizing the absolute value to underscore the biosensor's sensitivity to relative changes rather than absolute metrics.

$$S_{SS} = \left| \left(\frac{SS_{(air)} - SS_{(bio)}}{SS_{(air)}} \right) * 100 \right| \quad \ldots(2)$$

3.3 Effect of Unequal Source and Drain Doping

To explore the effects of differing doping levels, the source and drain doping are independently adjusted (varied). A reference doping level (RD) is set with the channel doping equals to $1*10^{10}/cm^3$ and drain/source doping equals to $1*10^{19}/cm^3$. When the drain doping is increased beyond the reference level, channel as well as source doping remains unchanged. Conversely, while increasing the source doping above the reference level, channel as well as drain doping are held constant. Table 4 outlines the specific doping levels for D_{D1}-D_{D3}, D_{RD}, and D_{S1}-D_{S3}.

Increasing N_D above the reference level reduces the effective channel length, requiring less gate voltage to activate the device and resulting in a lower threshold voltage. Figure 12 displays how the threshold voltage varies without and with biomolecules. Biomolecules increase the threshold voltage due to the formation of a strong lateral electric field across the channel. Consequently, the fractional change $|V_{t(air)} - V_{t(bio)}|/V_{t(air)}$ increases as drain doping levels rise. This relationship is visually represented in Fig. 13, which illustrates the sensitivity of threshold voltage variation with respect to N_D.

As N_D increases beyond the reference level, the depletion region extends further into the channel at the drain junction[29,31]. This extension results in a reduction of the depletion capacitance (C_{dep}), leading to a decrease in the subthreshold swing while increasing the subthreshold slope. Figure 14(a) illustrates this trend. Additionally, Fig. 14 (b) shows that the fractional change $|SS_{(air)}–SS_{(bio)}|/SS_{(air)}$ increases as the drain doping level exceeds the reference doping.

As previously mentioned, when N_S is increased, Fig. 12 illustrates a decrease in the threshold voltage. The fractional change $|V_{t(air)} - V_{t(bio)}|/V_{t(air)}$ increases with higher source doping levels, as shown in Fig. 13. Furthermore, high N_S lead to a deeper penetration of the depletion region at the source-channel junction into the channel. This diminishes the C_{dep}, causing an increase in the subthreshold slope, as depicted in Fig. 14(a). Additionally, Fig. 14(b) illustrates that the subthreshold slope sensitivity also rises with

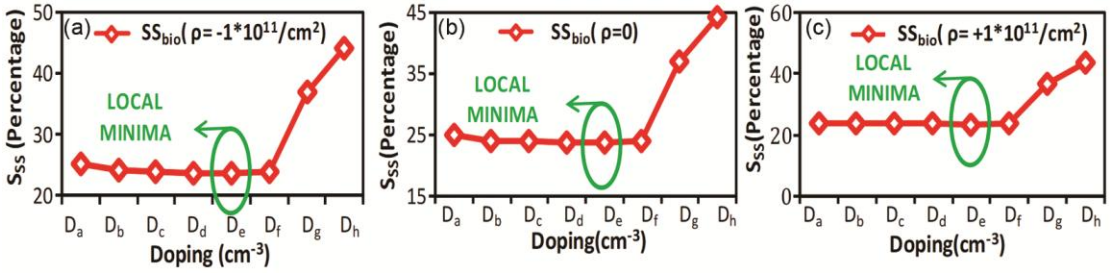

Fig. 11 — S_{SS} variation in the NWM-BD for (a) negatively charged (ρ=-1*10^{11}/cm^2), (b) neutral (ρ=0), and (c) positively charged (ρ=+1*10^{11}/cm^2) biomolecules at different doping (V_{DS}=0.5V, N_C=10^{10}/cm^3& K_{bio}=5)

Table 4 — Threshold voltage sensitivity & subthreshold slope sensitivity at different doping

	Doping (cm^{-3}) Source_Channel_Drain		Threshold Voltage Sensitivity (S_{Vt} : Percentage) — k_{bio} = 5			Subthreshold Slope Sensitivity (S_{SS} : Percentage) — k_{bio} = 5		
			ρ -1*10^{11} cm^{-2}	ρ 0	P +1*10^{11} cm^{-2}	ρ -1*10^{11} cm^{-2}	ρ 0	P +1*10^{11} cm^{-2}
D_{S3}	5*10^{20}_1*10^{10}_1*10^{19}	N_S ↑	96.4704	90.7895	85.0216	40.5620	40.4209	40.2651
D_{S2}	1*10^{20}_1*10^{10}_1*10^{19}		90.9764	85.4632	79.8665	39.5316	39.4166	39.3125
D_{S1}	5*10^{19}_1*10^{10}_1*10^{19}		87.5628	81.7503	76.6425	39.1903	39.1074	39.0235
D_{RD}	1*10^{19}_1*10^{10}_1*10^{19}	RD	74.1571	68.6916	63.0684	37.1150	36.9970	36.8762
D_{D1}	1*10^{19}_1*10^{10}_5*10^{19}		95.5378	89.2265	82.7258	40.8841	40.7662	40.6425
D_{D2}	1*10^{19}_1*10^{10}_1*10^{20}	N_D ↓	101.5939	95.0392	88.2835	41.4526	41.3113	41.1651
D_{D3}	1*10^{19}_1*10^{10}_5*10^{20}		110.4973	103.582	96.4543	42.1210	42.0127	41.9018

increasing N_S compared to the reference doping. In MOSFEBs, high doping in the source and low doping in the channel enhance charge carrier transport due to a reduced energy band gap. This doping configuration also increases the tunneling probability, altering the potential barrier at the source-channel junction, which is dependent on the electric field and gate/drain voltage. As a result, there is a larger current variation for the same range of applied voltage. The sensitivity of nanowire MOSFEB detector to biomolecules is attributed to the dependence of drain current, threshold voltage, and subthreshold swing on the source-to-channel potential barrier.

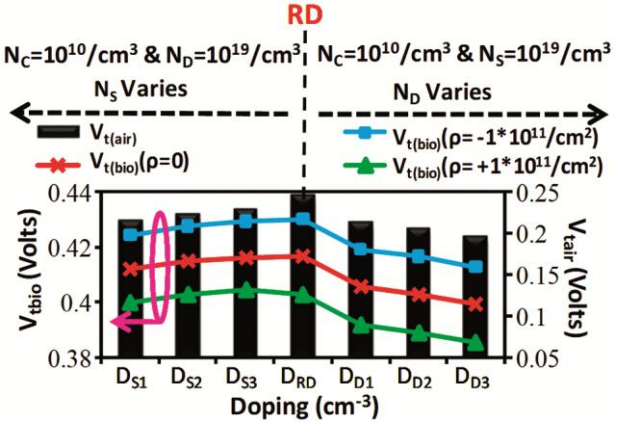

Fig. 12 — V_t variation in the NWM-BD when the cavity is filled with air and biomolecules (k_{bio}=5, N_C=10^{10}/cm^3& V_{DS}=0.5V)

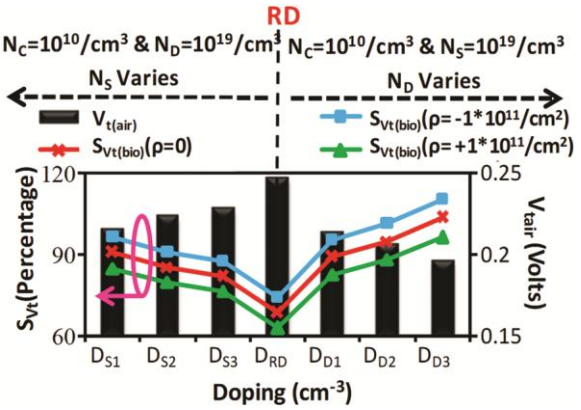

Fig. 13 — S_{Vt} in the NWM-BD for asymmetric doping variation (k_{bio}=5, N_C=10^{10}/cm^3& V_{DS}=0.5V)

Table 4 details the sensitivity of subthreshold slope and threshold voltage to different bio-chemical species under different drain/source doping conditions. Figure 15 illustrates the relative changes in subthreshold slope (ΔSS) as well as threshold voltage (ΔV_t) calculated at various doping levels. The findings highlight that negatively charged biomolecules exhibit pronounced ΔSS as well as ΔV_t absolute values, particularly at higher doping levels. As a sensitivity measure, threshold voltage yields a greater percentage sensitivity and relative change compared to subthreshold slope, rendering it more suitable for biosensing applications. Figure 16 depicts the variation in drain current (I_{DS}) at different doping, indicating enhanced current generation with increased doping due to the additional charge carriers generation.

Figure 17 illustrates the impact of V_{DS} on S_{SS} and S_{Vt} under symmetric and asymmetric doping conditions. For symmetric doping (SD), low source/drain doping (N_D=N_S=10^{19}/cm^3, N_C=10^{10}/cm^3) and high source/drain doping (N_D=N_S=10^{14}/cm^3, N_C=10^{10}/cm^3) are analyzed to observe the effects of drain biasing on sensitivity. Symmetric case (SD) features high doping (N_D=N_S=10^{19}/cm^3) and low doping (N_D=N_S=10^{14}/cm^3) levels, while asymmetric case (ASD) involves differing levels for the source and drain (N_D=10^{19}/cm^3, N_S=10^{20}/cm^3). Increasing the drain voltage correlates with increased S_{SS} and S_{Vt}. The observed increase in S_{SS} and S_{Vt} with rising V_{DS} can be attributed to the enhanced lateral electric field, which amplifies the impact of biomolecule-induced surface charge modulation on the channel

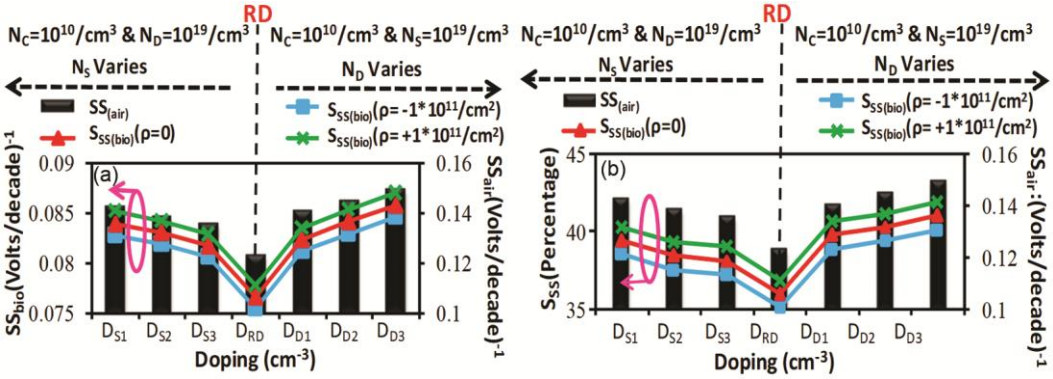

Fig. 14 — (a) SS, and (b) S_{SS} in the NWM-BD when the cavity is filled with biomolecules (k_{bio}=5, N_C=10^{10}/cm^3& V_{DS}=0.5V)

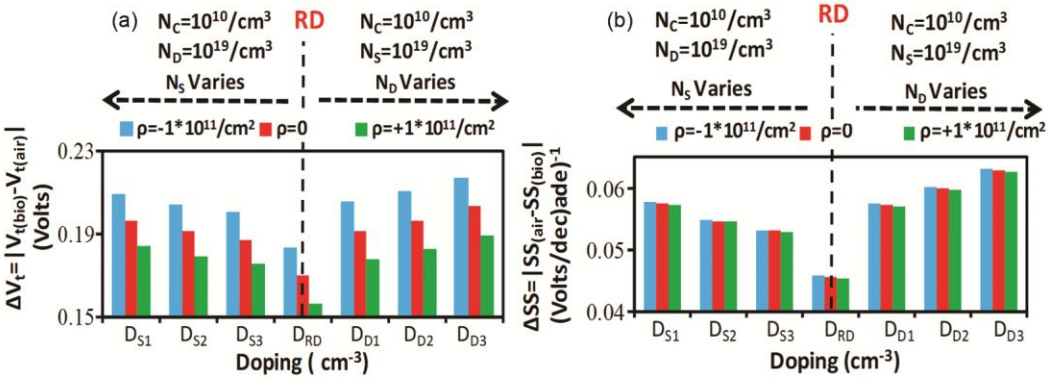

Fig. 15 — (a) Threshold voltage change, and (b) subthreshold slope change at different doping

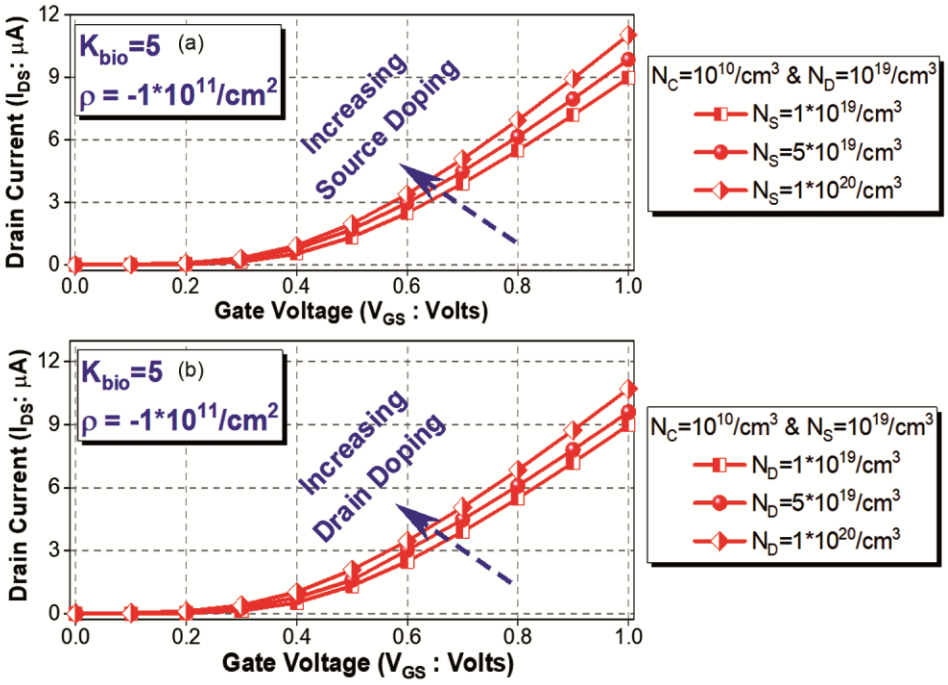

Fig. 16 — Drain current variation at different (a) N_S, and (b) N_D at V_{DS}=0.5V in NWM-BD

characteristics[24,32]. However, it is crucial to avoid exceeding a specific drain voltage limit to prevent device damage and ensure operational integrity. While higher V_{DS} generally improves sensitivity, it's important to note that this comes at the cost of increased power consumption and potential thermal effects, necessitating a careful balance in practical biosensing applications.

Table 5 shows the shift in the values of SS and V_t, which shows a higher relative change at high doping. It is quite evident from the above discussion that higher percentage change is obtained at low doping, whereas higher relative change is obtained at high doping. But, it should be kept in mind that conductivity is quite less at low doping and tunneling effect becomes prevalent at very high doping. Hence, an optimized doping should be considered for MOSFEB before fabrication. It is also interesting to note that the relative change or shift in the value of metric is a more reliable parameter in assessing the sensitivity of a MOSFEB detector. Relative change indicates the true value whereas percentage change indicates the relative fraction (modulated value) of the sensitivity.

3.4 Effect of Steric Hindrance and Cavity Dimensions

Steric hindrance is an important limiting factor in practical biosensors, resulting in a non-unity fill-in factor. The fill-in factor refers to the fraction of the total volume inside the cavity that is filled by the

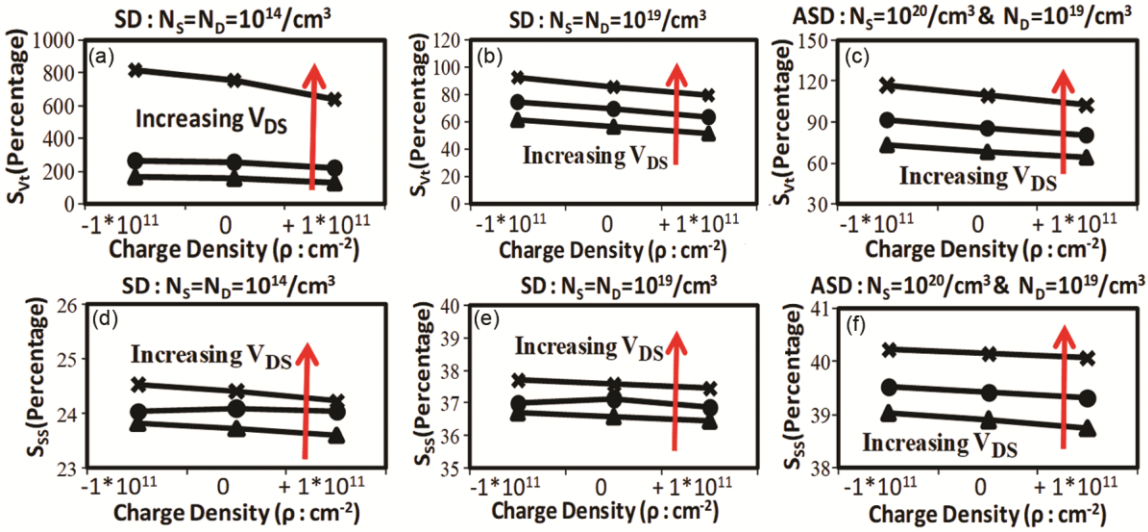

Fig. 17 — Impact of V_{DS} on (a-c) S_{Vt}, and (d-f) S_{SS} at different doping (k_{bio}=5, N_C=10^{10}/cm^3& V_{DS}=0.5V) in NWM-BD

Table 5 — Shift in sensing metrics in NWM-BD

Doping	Change in V_t (mV)		
	A	B	C
D_a	37.61747	37.06267	34.64357
D_b	52.4069	46.0499	37.0029
D_c	78.916	76.301	49.527
D_d	80.851	78.024	52.466
D_e	102.368	88.001	58.86
D_f	112.342	95.428	73.781
D_g	183.228	169.724	155.83
D_h	235.797	223.605	211.236
A : K_{bio}=5 & ρ= -1*10^{11}/cm^2	B : K_{bio}=5 & ρ= 0		C : K_{bio}=5 & ρ= +1*10^{11}/cm^2

biomolecules. The effect of steric hindrance is usually studied by considering different fill-in factors (such as horizontal or lateral filling) or fill-in profiles. Steric hindrance is a practical problem that arises from the partial hybridization of biomolecules. As a result, biomolecules only occupy a fraction of the cavity, impeding further filling of the remaining portion of the cavity. Hence, its effect must be thoroughly studied. Table 6 illustrates the impact of biomolecule location at different fill-in factors (horizontal filling) by dividing the cavity on both sides of the source and drain into four parts. Although a high fill-in factor generally results in high sensitivity[4] due to the immobilization of a large number of biomolecules, the location of the biomolecules significantly influences sensitivity, especially in partially filled cavities. For instance, although the fill-in factor of case 5 is more significant (higher) than that of case 4, the sensitivity in case 4 is higher, and the same observation can be made for other cases, such as case 10 and case 11. The influence of fill-in factor and profile on sensitivity underscores the importance of considering nano-scale phenomena in macroscopic device performance.

The fill-in factor of case 1 and case 4 are the same, but the location of the biomolecules is different in both cases. In case 1, the biomolecules are located near the source, resulting in higher sensitivity. This is because the threshold voltage is mainly affected by the potential hill appearing at the source-channel junction[28], and the biomolecules near the source affect this potential hill more than when they are near the drain. Similar observations can be made for other cases, such as case 5 and case 10, case 11 and case 14. The observed variations in sensitivity across different fill-in profiles offer valuable insights for developing computational models to predict and enhance biosensor responses. In the era of machine learning, these insights are crucial, as artificial intelligence can be harnessed to accurately predict and improve the sensitivity of biodetectors.

Figure 18 shows the effect of the fill-in factor (lateral filling), and Fig. 19 depicts how different fill-in profiles affect the threshold voltage sensitivity. These findings underscore the need for precise control over biomolecule immobilization techniques to achieve desired fill-in patterns and optimize sensor performance. A higher fill-in factor directly correlates with the increased sensitivity. The fill-in profile refers to the pattern filled by biomolecules within the cavity, with a symmetrical fill-in profile considered on both sides of the cavity. The concave fill-in profile has demonstrated the highest sensitivity compared to

Table 6 — Effect of fill-in factor and location of biomolecules on sensitivity

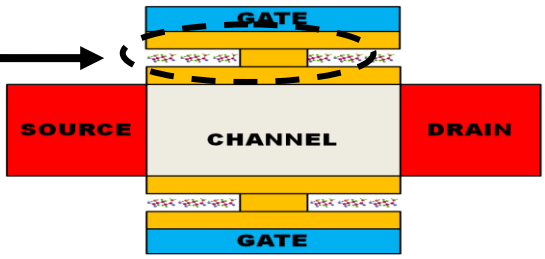

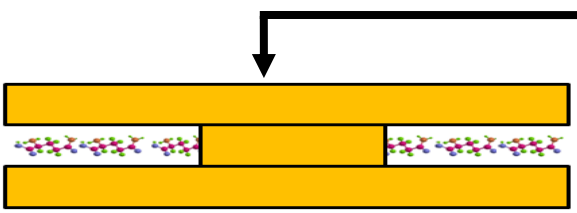

Cavity on both sides is divided into two equal parts

S. No.	Cavity towards the source end L_1	Oxide layer L_{EOX}	Cavity towards the drain end L_2	Fill-in Factor	Threshold voltage shift (ΔV_t : mV) Biomolecules A	B	C
1.				0.25	26.826	14.449	1.026
2.				0.25	31.991	19.004	6.283
3.				0.25	84.910	72.028	58.297
4.				0.25	113.878	98.452	89.193
5.				0.50	35.024	24.557	11.134
6.				0.50	90.034	77.421	64.212
7.				0.50	93.779	80.496	67.862
8.				0.50	117.928	102.665	93.298
9.				0.50	121.392	106.772	97.421
10.				0.50	171.376	157.682	142.299
11.				0.75	99.783	86.032	73.016
12.				0.75	130.081	115.491	102.613
13.				0.75	177.832	163.991	149.002
14.				0.75	179.083	165.842	150.991

A : K_{bio}=5 & ρ= -1*10^{11}/cm^2 B : K_{bio}=5 & ρ= 0 C : K_{bio}=5 & ρ= +1*10^{11}/cm^2

Presence of biomolecules Absence of biomolecules Oxide layer (SiO_2)

N_S=10^{19}/cm^3 , N_D=10^{19}/cm^3 , N_C=10^{10}/cm^3

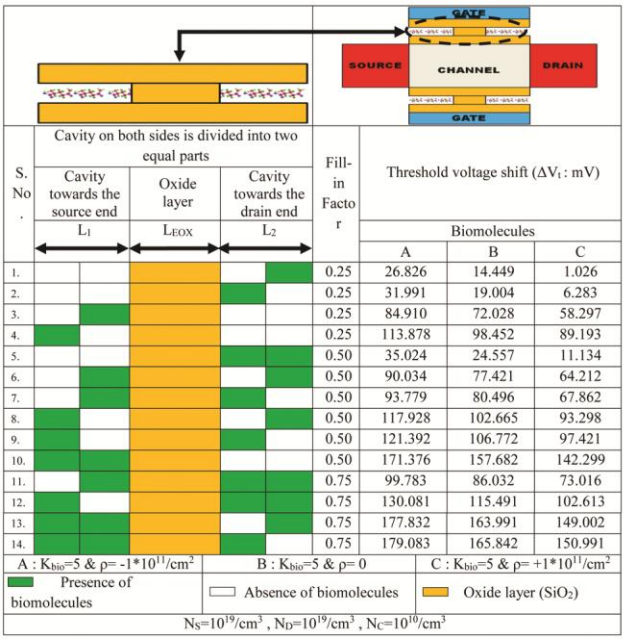

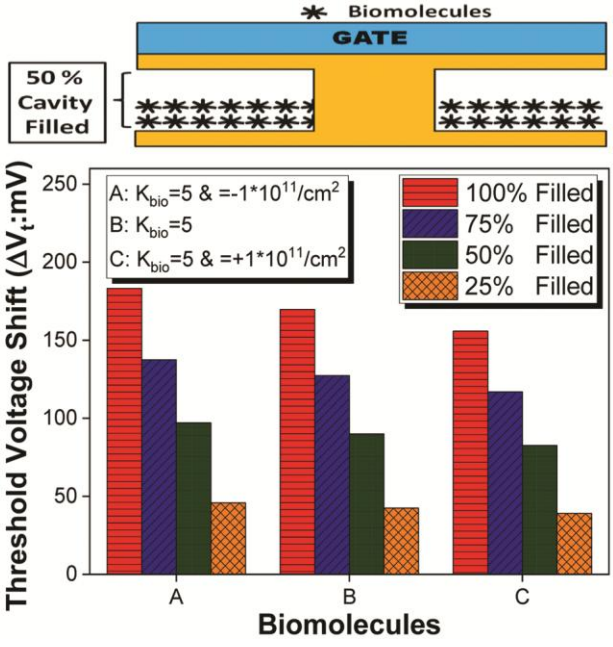

Fig. 18 — Impact of fill-in factor on sensitivity in NWM-BD

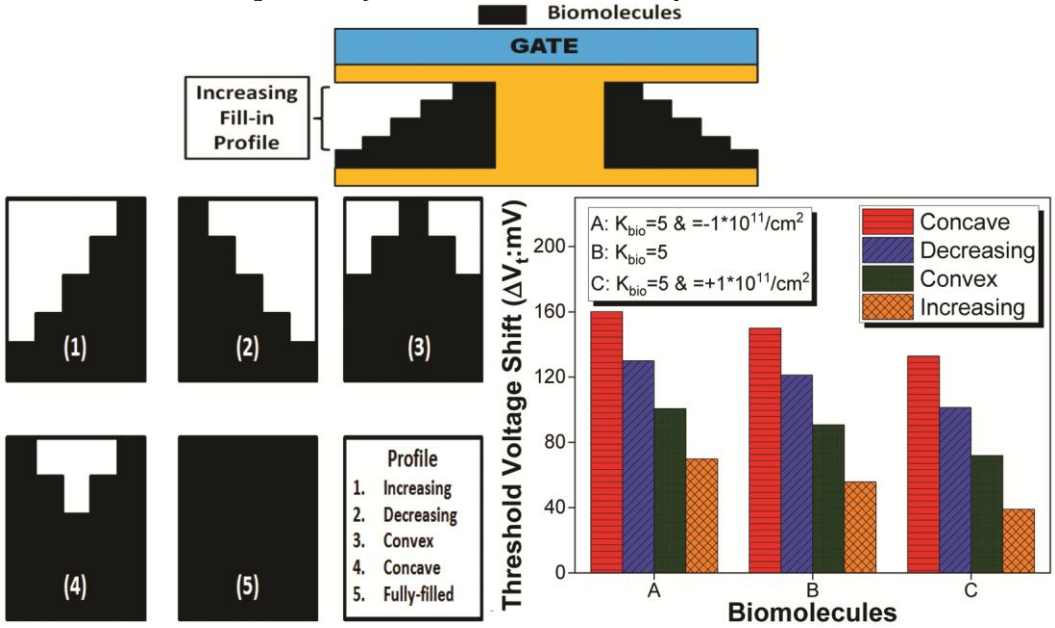

Fig. 19 — Impact of different fill-in profiles on sensitivity

Table 7 — Effect of cavity dimensions on sensitivity in NWM-BD

Parameter		Threshold voltage shift (ΔV_t : mV) A	B	C
Cavity Length (L_1=L_2)	14 nm	183.228	169.724	155.838
	12 nm	165.892	151.921	137.296
	10 nm	142.769	127.992	113.877
	08 nm	105.921	86.256	74.523
Cavity Thickness (t_{CAV})	02 nm	183.228	169.724	155.838
	04 nm	196.772	181.997	167.826
	06 nm	212.911	196.285	182.719
	08 nm	235.616	218.983	205.912

A : K_{bio}=5 & ρ= -1*10^{11}/cm^2 C : K_{bio}=5 & ρ= +1*10^{11}/cm^2
B : K_{bio}=5 & ρ= 0

other fill-in profiles. This sensitivity is due to the accumulation of biomolecules near the source-channel junction, which enhances the coupling between the gate and channel. As a result, the biomolecules near the source exerts stronger control over the flow of charge carriers, thereby increasing sensitivity. Further investigation into the kinetics of biomolecule immobilization and their spatial distribution within the cavity could lead to innovative strategies for improving sensor sensitivity and specificity.

Table 7 displays the impact of cavity thickness/length on sensitivity. The relationship between cavity dimensions and sensitivity underscores the importance of optimizing the sensing area in MOSFET-based biosensors. An increase in

Table 8 — Impact of parameters on sensitivity

Parameters		Threshold voltage shift (ΔV_t : mV) A	B	C
Radius of Channel (a: nm)	10	183.228	169.724	155.838
	11	169.491	155.669	141.287
	12	155.002	140.928	126.882
Operating Temperature (T: K)	250	178.982	164.509	151.008
	300	183.228	169.724	155.838
	350	189.945	175.672	160.429

A : K_{bio}=5 & ρ= -1*10^{11}/cm^2 C : K_{bio}=5 & ρ= +1*10^{11}/cm^2
B : K_{bio}=5 & ρ= 0

cavity size results in elevated sensitivity levels for both threshold voltage and subthreshold slope. This is due to the greater number of charge carriers immobilized within the cavity, which enhances the device's sensitivity to biomolecules. Further investigation could explore whether there's an optimal cavity size beyond which sensitivity gain diminishes, balancing performance with practical fabrication constraints.

Table 8 presents the influence of channel radius and temperature on the sensitivity. It is observed that as the channel radius increases, the sensitivity decreases. This reduction in sensitivity is attributed to the diminished control of the gate over the channel, primarily caused by the decrease in capacitive coupling. This trade-off between channel size and

sensitivity suggests that optimizing device geometry is crucial for balancing performance with manufacturability. However, it is important to note that the number of intrinsic charge carriers also increases with the increasing temperature, which leads to an increase in sensitivity. Therefore, while increasing the channel radius may have a negative impact on sensitivity due to reduced gate control, the increase in intrinsic charge carriers (due to an increase in temperature) counters this effect and contributes to an overall increase in sensitivity. The temperature dependent sensitivity increases underscores the need for precise temperature control in biosensing applications to ensure consistent and reliable measurements

3.5 Effect of Material Engineering

Material engineering also enhances the sensitivity of nanowire MOSFEB detectors[4]. Basically, material engineering refers to the i) use of different source/drain materials, ii) use of multi-gate architecture, iii) use of graded channel engineering, and iv) use of gate oxide stacking.

3.5.1 Source/Drain Engineering

Table 9 presents the threshold voltage sensitivity (threshold voltage shift) resulting from the use of different drain/source materials. This analysis examines how the conventional material, silicon, compares to alternative materials. The selection of drain/source materials also influences the device's resistance to biofouling and chemical degradation, factors that are essential for long-term stability in biological environments. This factor is crucial, as altering the drain and source materials affects the potential barrier at both the drain and source junctions. These junctions are pivotal since the charge carriers contributing to the total current are significantly influenced by these barriers at the channel-drain and channel-source interfaces. Among all the materials tested, silicon shows the highest sensitivity. Generally, materials with lower bandgaps are more sensitive to biomolecular interactions, whereas those with larger bandgaps exhibit more significant relative changes in sensing metrics[4,6,33,34]. However, each has its disadvantages: lower bandgap materials tend to increase leakage current (leading to false turn-on of the detector) and have lower breakdown voltages, while higher bandgap materials pose fabrication challenges due to high defect density and low carrier mobility, limiting their use in high-speed applications[4,34]. The interface between the chosen drain/source material and channel plays a significant role in determining the overall device performance, highlighting the need for careful material selection and interface engineering.

Table 9 — Impact of different materials on sensitivity in NWM-BD

Material			Biomolecules		
Source	Drain	Bandgap (300 K)	A	B	C
Si	Si	1.1 eV	183.228	169.724	155.838
Ge	Ge	0.7 eV	138.007	112.942	93.721
GaAs	GaAs	1.42 eV	114.408	94.589	77.298
InP	InP	1.351 eV	119.287	103.669	81.870
InSb	InSb	0.18 eV	72.115	57.346	40.379
GaSb	GaSb	0.726 eV	172.390	145.498	126.571
InAs	InAs	0.36 eV	160.284	139.330	115.690

A : K_{bio}=5 & ρ= -1*10^{11}/cm^2 C : K_{bio}=5 & ρ= +1*10^{11}/cm^2
B : K_{bio}=5 & ρ= 0

It is noteworthy that sensitivity is not solely dependent on the bandgap of the semiconductor material. Other factors, such as electron mobility, electron affinity, charge carrier density and doping profiles, also play crucial roles. Therefore, all these factors must be carefully analyzed before selecting the material for the source and drain. In general, materials with lower bandgaps have lower energy bandgaps but higher electron and hole mobility, whereas materials with higher bandgaps have higher energy bandgaps but lower mobility of electrons and holes. Consequently, silicon's sensitivity remains the highest. In the following next sections, the focus shifts primarily to three materials, specifically those with lower energy bandgaps: silicon, germanium, and indium arsenide (InAs). Germanium is considered one of the best alternatives to silicon, despite its disadvantages[35], while InAs is another promising compound semiconductor material with high potential for use in biosensor detectors[36,37].

3.5.2*Oxide Engineering*

Figure 20 demonstrates the influence of gate oxide stacking on threshold voltage sensitivity at t_1=1nm and t_2=3nm. It can be observed that sensitivity is increased when SiO_2 and high-K dielectric are stacked. The observed increase in sensitivity with gate oxide stacking can be attributed to the improved capacitive coupling between the gate and the channel, allowing for more effective modulation of the channel conductivity by biomolecular interactions[38]. The choice of high-K material and its thickness ratio with

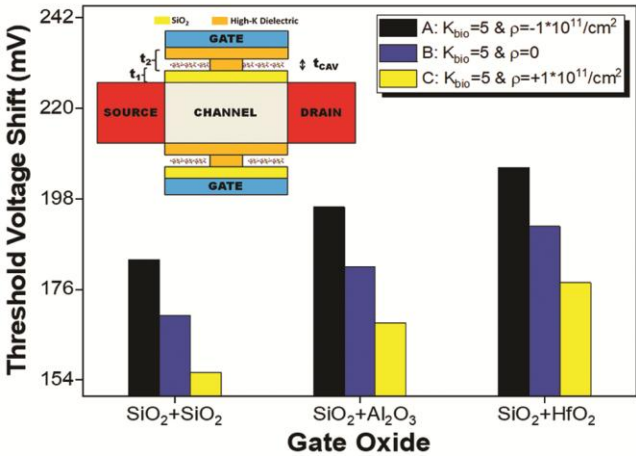

Fig. 20 — Effect of gate-oxide stacking on sensitivity in NWM-BD

SiO_2 can be further optimized to balance sensitivity gains with overall device performance and reliability. However, it is essential to remember that this approach also increases fabrication complexity, as high-k dielectric deposition is subject to certain limitations[8]. The increased fabrication complexity associated with high-K deposition might be mitigated by emerging deposition techniques or alternative high-K materials that are more compatible with standard CMOS processes.

3.5.3*Gate and Channel Engineering*

Apart from doping and gate oxide stacking, sensitivity also increases due to dual gate architecture[39] and graded channel due to the enhanced electric field[40].To study the impact of gate engineering on sensitivity, dual gate architecture has been considered in nanowire MOSFEB with equal gate length for both gates (rest, all the parameters have been considered the same). The work function of gate-1 and gate-2 are ϕ_{G1} and ϕ_{G2} respectively. The work function of gate-1 (near to source) is greater than that of gate-2 (near to drain) so as to obtain high sensitivity[28]. The work function difference between the gates creates a built-in electric field along the channel, which can be optimized to enhance the device's response to biomolecular interactions. Reversing the value of the work function decreases the sensitivity of the biosensor since a high work-function gate effectively modulates the flow of charge carriers by controlling the source-channel potential barrier. As discussed in the previous section, the source-channel barrier highly affects the sensitivity as compared to the drain-channel potential barrier. The dual gate architecture not only improves sensitivity but also offers better control over the channel, potentially reducing short-channel effects in nanoscale devices. While dual gate architecture offers improved sensitivity, it's important to consider the trade-offs in terms of fabrication complexity and potential increase in parasitic capacitances[14,41,43].

For considering the effect of channel engineering, a dual-step graded doping profile has been considered for the channel. The channel has been divided into two equal parts with doping of N_{CH1} (part of the channel near to source) and N_{CH2} (part of the channel near to source). Lateral step-graded doping in the channel enhances the sensitivity by creating a doping gradient that improves charge carrier mobility. This gradient facilitates faster charge transport and increases the effective carrier concentration, resulting in enhanced current and voltage modulation[40]. Consequently, sensitivity increases due to the step-graded doping profile. Keeping $N_{CH2}>N_{CH1}$, the potential barrier at the source junction is lower (compared to the drain junction), which facilitates smooth transportation of charge carriers, and hence, high sensitivity is obtained when compared to the case where $N_{CH1}>N_{CH2}$[40]. The dual-step graded doping profile not only improves sensitivity but also helps in mitigating short-channel effects, which is crucial for scaling down device dimensions. While step-graded doping improves sensitivity, it's important to consider the challenges in precisely controlling doping profiles at nanoscale dimensions and their potential impact on device-to-device variability[44]. Table 10 shows the percentage improvement in sensitivity due to gate and channel engineering. Future research could explore more complex graded doping profiles, such as continuous gradients or multi-step profiles, to further enhance sensitivity and device performance.

3.6 Impact of Trap Charges, Cavity Location, and LOD

The device reliability is affected mainly by various factors, including trap charges (can adversely impact device performance by altering the electrical characteristics leading to inaccurate biosensor readings), off-current, and hot carrier injection.Trap charges in the gate oxide can lead to shifts in the threshold voltage and degradation in device performance over time. Trap charges may occur in the device as a result of defects during the manufacturing process. These interface trap charges decrease the device's reliability and accelerate the aging mechanism. Different source materials may exhibit varying susceptibilities to trap charges formation,

Table 10 — Impact of gate and channel engineering on sensitivity

Bio Molecules	ΔV_t (mV) With GE	ΔV_t (mV) Without GE	% Improvement
GE: Gate-Engineering ($L_G=L_{G1}+L_{G2}$ & $L_{G1}=L_{G2}$) ϕ_{G1}=5.1 eV[45] and ϕ_{G2}=4.1 eV[46]			
A	212.291	183.228	15.861
B	198.811	169.724	17.137
C	184.782	155.838	18.573
GE: Gate-Engineering ($L_G=L_{G1}+L_{G2}$ & $L_{G1}=L_{G2}$) ϕ_{G1}=4.1 eV[46] and ϕ_{G2}=5.1 eV[45]			
A	191.910	183.228	4.738
B	178.204	169.724	4.996
C	162.995	155.838	5.234

Bio Molecules	ΔV_t (mV) With CE	ΔV_t (mV) Without CE	% Improvement
CE: Channel-Engineering ($L_{CH}=L_{CH1}+L_{CH2}$ & $L_{CH1}=L_{CH2}$) $N_{CH1}=10^{10}/cm^3$ and $N_{CH2}=10^{15}/cm^3$			
A	204.577	183.228	11.651
B	190.004	169.724	11.948
C	176.813	155.838	13.459
CE: Channel-Engineering ($L_{CH}=L_{CH1}+L_{CH2}$ & $L_{CH1}=L_{CH2}$) $N_{CH1}=10^{15}/cm^3$ and $N_{CH2}=10^{10}/cm^3$			
A	189.001	183.228	3.150
B	175.618	169.724	3.472
C	161.279	155.838	3.812

A : K_{bio}=5 & ρ= -1*10^{11}/cm^2 C : K_{bio}=5 & ρ= +1*10^{11}/cm^2

B : K_{bio}=5 & ρ= 0

influencing the choice of materials for specific biosensing application. The impact of different interface trap charges (assumed across the length L_{EOX} across the oxide channel interface at doping $N_D=N_S=10^{19}/cm^3$ and $N_C=10^{10}/cm^3$) has been examined across various source materials for K_{bio}=5 in Table 11.

Mitigation strategies, such as optimized annealing processes or the use of high-quality interfacial layers, can help reduce the impact of trap charges on device reliability. Both positive and negative interface trap charges ($\pm$ 1*10^{12}/cm^2) have been considered on the channel-oxide interface[47]. Notably, the silicon source material has demonstrated superior reliability (lowest change in threshold voltage due to trap charges). The gate-all-around architecture also proven effective in mitigating several short-channel effects compared to the planar architecture. Hot carrier injection (causes oxide breakdown) is an undesired effect that affects long-term reliability. This is mainly due to the high electric field near the drain end. Table 12 displays the

Table 11 — Impact of trap charges on sensitivity

Source Material	Trap Charges	ΔV_t (mV)	Change in ΔV_t (mV)
	WPITC	166.992	2.732
Si	WITC	169.724	-
	WNITC	171.289	1.565
	WPITC	168.529	5.447
Ge	WITC	173.976	-
	WNITC	178.825	4.849
	WPITC	170.091	6.791
InAs	WITC	176.882	-
	WNITC	182.239	5.357

WPITC: With Positive Interface Trap Charges
WITC: Without Interface Trap Charges
WNITC: With Negative Interface Trap Charges

Table 12 — Peak electric field and off-current variation for different source materials

Source Material	Peak-Field (V/m)	I_{OFF} (pA)
Si	1.411*10^6	75.552
Ge	1.936*10^6	131.029
InAs	2.891*10^6	152.998

peak electric field near the drain end and off-current at V_{GS}=0V and V_{DS}=1V for K_{bio}=5. Excessive off-current contributes to power wastage and reduced overall device reliability.It can be seen that silicon has a lower off-current (due to its high band gap) and low electric field compared to other materials. Hence, the silicon is more reliable than other materials.

The limit of detection (LOD) refers to the minimum concentration of a biochemical species that a biosensor can detect. The analytical assessment of LOD involves the application of curve fitting and regression analysis techniques[48,49]. LOD is determined by analyzing the drain current sensitivity response for K_{bio}=5. In Fig. 21, the plot demonstrates the relationship between the fractional change in drain current ($\Delta I_{DS}/I_{DS}$) and the varying concentration range of the biomolecule within the cavity, spanning from 0.0001 to 1000 mg/ml. The inset compares the LOD of nanowire MOSFEB detector using different source materials. It is observed that the LOD obtained for the silicon source is approximately 11.61 / 27.24% higher than the LOD obtained for Ge/InAs source. Moreover, the stability and repeatability of the sensor's performance over multiple uses and different environmental conditions are critical aspects that ensure consistent and dependable detection capabilities. Continuous advancements in material science and nanotechnology contribute to the development of more efficient and precise biosensors,

further pushing the boundaries of LOD and enhancing their practical applications in various fields.

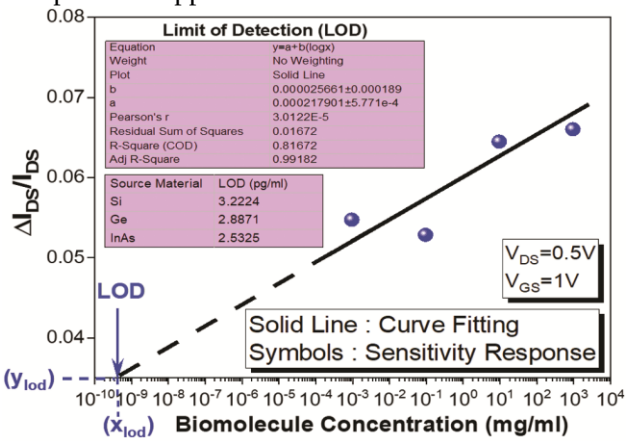

Fig. 21 — Current sensitivity response curve in NWM-BD

Table 13 — Impact of cavity location on sensitivity

Threshold voltage shift (ΔV_t : mV)					
Cavity Length			Biomolecules		
L_1 (nm)	L_{EOX} (nm)	L_2 (nm)	A	B	C
0	2	28	130.008	118.291	102.226
14	2	14	183.228	169.724	155.838
28	2	0	225.667	209.791	196.009

A : K_{bio}=5 & ρ= -1*10^{11}/cm^2 C : K_{bio}=5 & ρ= +1*10^{11}/cm^2
B : K_{bio}=5 & ρ= 0

Cavity location also plays a crucial role in affecting the sensitivity of nanowire MOSFEB detector. Table 13 shows the effect of cavity location on sensitivity (the aspect ratio is kept the same by keeping the total length L_1+L_{EOX}+L_2 constant). The biosensor is highly sensitive to biomolecules when the cavity is embedded near the source. As discussed in the previous section, biomolecules inside the cavity (near the source junction) effectively controls the flow of charge carriers via capacitive coupling[25, 50-51]. Hence, the biosensor becomes more sensitive to biomolecules. Advanced simulation and modeling techniques can aid in precisely determining the optimal cavity location and configuration to achieve the highest sensitivity and selectivity. These considerations are vital for the development of next-generation biosensors with superior performance metrics.

3.7 Comparison with Junctionless Variant

Junctionless variants have fabrication advantage over the inversion type variants[52]. Here, in Fig. 22, the sensitivity of the nanowire MOSFEB has been compared with its junctionless variant. The proposed MOSFEB shows over ~95mV improvement over the

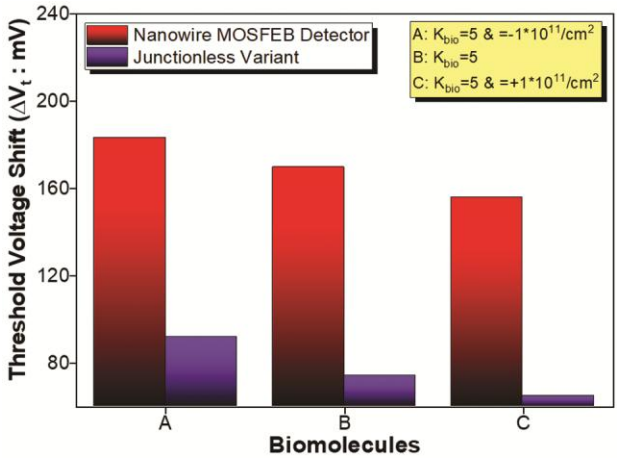

Fig. 22 — Comparison of NWM-BD with its junctionless variant

junctionless variant for K_{bio}=5. And the same trend can be seen for the charged biomolecules also. For junctionless variant, the doping and type of the semiconductor material used in this analysis is same for source/channel/drain (doping considered here is 10^{19}/cm^3).

Junctionless FET based-biosensors typically exhibit lower sensitivity in terms of threshold voltage changes compared to conventional inversion-mode FETs due to their distinct operating principles[53,54]. While inversion-mode MOSFETs rely on surface conduction in a thin inversion layer, junctionless MOSFETs operate through bulk conduction in a heavily doped channel. This bulk conduction mode makes junctionless devices less sensitive to surface charge changes induced by biomolecule interactions or localization inside the cavity. Additionally, the weaker gate control and reduced electrostatic coupling in junctionless devices result in a smaller impact on the threshold voltage when biomolecules interact with the detector[15]. Consequently, the threshold voltage in junctionless devices is less responsive to the presence of bio-chemical species, leading to lower sensitivity compared to their inversion-mode counterparts. Despite their lower threshold voltage sensitivity, junctionless MOSFET biosensor offers potential advantages in terms of simpler fabrication processes, reduced short-channel effects, and potentially lower noise levels, which can be beneficial in certain biosensing applications where these factors are prioritized over absolute sensitivity[1].

3.8 Sensitivity Analysis for Different Biomolecules

Different biomolecules have significance in the biomedical field. Biomolecules such as Uricase (K_{bio}=1.54), Streptavidin (K_{bio}=2.1), Biotin

Table 14 — Threshold voltage shift for different neutral biomolecules

Biomolecules	Reference	Sensitivity ΔV_t (mV)	Sensitivity S_{Vt} (Percentage)
Uricase	12	65.54873	26.529
Streptavidin	12	97.0815	39.291
Biotin	40	118.595	47.998
APTES	12	140.6225	56.913
Hydroprotein	15	169.724	68.691
Keratin	9	207.2831	83.892
Gelatin	24	254.7775	103.114

Table 15 — Benchmarking the performance of NWM-BD detector with similar biosensors

Structure	K_{bio}	S_{Vt} (V)	Reference
NWM-BD (Our Work)	12	0.2547	-
GaN-GME-DE-SNW-FET	8	0.1050	9
TGRC-MOSFET	8	0.0072	55
QG-MC-MOSFET	12	0.1610	56
TGAA-NWFET	2.1	0.0172	57

(K_{bio}=2.63), ChOx (K_{bio}=3.3), APTES (K_{bio}=3.57), Keratin (K_{bio}=8) and Gelatin (K_{bio}=12) are some of the commonly used neutral biomolecules.The sensitivity of the biosensor increases with the increasing dielectric constant (K_{bio}). High K_{bio} increases the coupling between the charge carriers and gate via capacitive coupling. Hence, the sensitivity increases with increasing K_{bio}. Table 14 presents the sensitivity comparison for these biomolecules. Table 15 is a benchmark for comparing the performance of nanowire MOSFEB detector to that of similar biosensors.

Label-free biosensors, including NWM-BD, inherently face challenges in achieving high selectivity. While our biosensor exhibits high sensitivity to the target analyte, selectivity can be enhanced by incorporating selective recognition elements, such as a bioreceptor layer, though this may increase fabrication complexity and reduce sensitivity. As selectivity remains a fundamental challenge in label-free biosensors, sensitivity is often the primary benchmark. The nanosensor (NWM-BD) functions by immobilizing biomolecules within a nanogap cavity, requiring advanced fabrication techniques for precise nanoscale dimensions, adding complexity to the process. However, the proposed nanosensor offers high sensitivity and cost-effectiveness compared to conventional biosensors, making it promising for label-free biosensing. Despite its high sensitivity, its selectivity is relatively low but can be improved with an additional bioreceptor layer at the cost of increased fabrication complexity. Additionally, repeated usage may cause wear and tear, potentially reducing the sensor's operational lifetime and reusability.

4 Conclusion

This paper presents a comprehensive sensitivity analysis of a nanowire-based MOSFEB detector, focusing on the impact of doping on sensitivity. The uniqueness of this study lies in its methodology, which investigates sensitivity enhancement through doping modulation and the effect of partially filled cavities (steric hindrance) at different fill-in factors and profiles. Both relative and percentage sensitivity are considered in the sensitivity exploration. The findings indicate that sensitivity exhibits a greater percentage change at lower doping levels, while the relative change peaks at higher doping levels. Various parameters, including cavity dimensions, material engineering, drain voltage, operating temperature, oxide stacking, source material, and channel radius, significantly influence sensitivity. The analysis of steric hindrance reveals that the location of biomolecules impacts sensitivity more than their fill-in factor. The detector shows a sensitivity enhancement of approximately 95.716 mV over its junctionless variant (for K_{bio}=5), with oxide and gate engineering techniques contributing more significantly to sensitivity enhancement than other engineering methods. The proposed biosensor achieves a limit of detection of 3.2224 pg/ml. Doping, bias, and biomolecule location are also the critical factors in determining sensitivity revealed through various simulated results. This work provides a valuable framework for studying and enhancing the sensitivity of similar biosensors, offering a thorough investigation into biosensing performance.

References

1 Sirohi A, Sahu C & Singh J, *IEEE Access*, 7 (2019) 141810.
2 Das A, Kanaujia B K, Nath V, Rewari S & Gupta R S, *IEEE 17th India Counc Int Conf INDICON*, (2020) 1.
3 Kaisti M, *Biosens Bioelectron*, 98 (2017) 437.
4 Das A, Rewari S & Kanaujia B K & Gupta R S, *Silicon*, 14 (2022) 5133.
5 Mendiratta N, Tripathi S L, *J Semicond*, 41 (2020) 061401.
6 Jianrong C, Yuqing M, Nongyue H, Xiaohua W & Sijiao L, *Biotechnol Adv*, 22 (2004) 505.
7 Syahir A, Usui K, Tomizaki K, Kajikawa K & Mihara H, *Microarrays*, 4 (2015) 228.
8 Chakraborty A & Sarkar A, *J Comput Electron*, 16 (2017) 556.

9 Sharma S, Nath V, Deswal S S & Gupta R S, *Microelectronics J*, 129 (2022) 105599.
10 Li J, Zhang Y, To S, You L & Sun Y, *ACS Nano*, 5 (2011) 6661.
11 Chiang M H, Lin C N & Lin G S, *Semicond Sci Technol*, 21 (2006) 190.
12 Pratap Y, Kumar M, Kabra S, Haldar S, Gupta R S & Gupta M, *J Comput Electron*, 17 (2018) 288
13 Yadav S & Rewari S, *Microsyst Technol*, 30 (2024) 565.
14 Kumari M, Singh N K & Sahoo M, *Sci Rep*, 12 (2022) 21115.
15 Goel A, Rewari S, Verma S, Deswal S S & Gupta R S, *IEEE Sens J*, 21(2021) 16731.
16 Das A, Kanaujia B K, Deswal S S, Rewari S & Gupta R S,*2022 IEEE Int Conf Electron Devices Soc Kolkata Chapter (EDKCON)*, (2022) 1.
17 Zhang Y, Han K & Li J, *Micromachines*, 11 (2020) 1.
18 Ganesh A, Goel K, Mayall J S & Rewari S, *Silicon*, 14 (2022) 4063.
19 Li C, Liu F, Han R & Zhuang Y, *IEEE Access*, 9 (2021) 63602.
20 Sze S M, Physics of semiconductor devices, (Wiley EasternLimited, New Delhi) 2nd Edn, (1983) 71.
21 Das A, Rewari S, Kanaujia B K, Deswal S S & Gupta R S, *Micro and Nanostructures*, 204 (2025) 208152.
22 Lodhi A, Rajan C, Kumar A, Dip B, Samajdar P & Soni D, *Appl Phys A*, 126 (2020) 837.
23 Rosini E, D'antona P & Pollegioni L, *Int J Mol Sci*, 21 (2020) 4574.
24 Yadav S & Rewari S, *Proc. 2022 IEEE Int. Conf. Electron Devices Soc. Kolkata Chapter (EDKCON), (2022)* 23.
25 Das A, Rewari S, Kanaujia B K, Deswal S S & Gupta R S, *Microelectronics J*, 138 (2023) 105832.
26 Yadav S & Rewari S, *Microelectronics J*, 142 (2023)106011.
27 Yadav S, Das A & Rewari S, *ECS J Solid State Sci Technol*, 13 (2024) 047001.
28 Kumari M, Singh N K, Sahoo M & Rahaman H, *Appl Phys A Mater Sci Process*, 127 (2021)1.
29 Adel SS, C.Smith K. 2020. *Microelectronics Circuit*. Oxford. 1296 pp. 8th ed.
30 Beckers A, Jazaeri F & Enz C, *IEEE Electron Device Lett*, 41 (2019) 276.
31 Kaul A, Rewari S & Nand D, *Microsyst Technol*, 30 (2024) 599.
32 Kaul A, Yadav S, Rewari S & Nand D, *IEEE Trans Dielectr Electr Insul*, (2025).
33 Bhat A M, Varghese A, Shafi N & Periasamy C, *IETE J Res*, 69 (2021) 1419.
34 Wadhera T, Kakkar D, Wadhwa G & Raj B, 2019. *J. Electron. Mater*, 48 (2019) 7635.
35 Lee H, Park J D & Shin C, *IEEE Trans Electron Devices*, 63 (2016) 1827.
36 Dey A W, *et al*., *IEEE Electron Device Lett*, 33 (2012) 791.
37 Swati, Kaur J & Singh A K, *Appl Phys A Mater Sci Process*, 129 (2023) 365.
38 Das A, Rewari S, Kanaujia B K, Deswal S S & Gupta R S, *J Comput Electron*, 22 (2023) 742.
39 Goel A, Rewari S, Verma S & Gupta R S, *Proc. Int. Conf. 2018 IEEE Electron Device Kolkata Conf EDKCON*, (2018) 337.
40 Das A, Rewari S, Kanaujia B K, Deswal S S & Gupta R S, *Int J Numer Model*, 36 (2023) e3106.
41 Darwin S & Arun Samuel T S, *Silicon*, 12 (2020) 393.
42 Kaul A, Rewari S & Nand D, *ECS J Solid State Sci Technol*, 13 (2024) 103010.
43 Barik M A, Deka R & Dutta J C, *IEEE Sens J*, 16 (2016) 280.
44 Singh K N & Dutta P K, *Superlattices Microstruct*, 155 (2021) 106897.
45 Das R, Chanda M & Sarkar C K, *IEEE Trans Electron Devices*, 65 (2018) 5487.
46 Kumar M, Haldar S, Gupta M & Gupta R S, *Superlattices Microstruct*, 111 (2017) 10.
47 Madan J & Chaujar R, *IEEE Trans Device Mater Reliab*, 16 (2016) 227.
48 Nuzaihan MMN, et al., *Biosens Bioelectron*, 83 (2016) 106.
49 Kaul A, Yadav S, Rewari S &Nand D, *Micro and Nanostructures*, 191 (2024) 207851.
50 Das A, Rewari S, Kanaujia B K, Deswal S S & Gupta R S, *Phys Scr*, 98 (2023) 115013.
51 Das A, Rewari S, Kanaujia B K, Deswal S S & Gupta R S, *Phys Scr*, 98 (2023) 074005.
52 Pratap Y, Kumar M, Kabra S, Haldar S, Gupta R S & Gupta M, *J Comput Electron*, 17 (2018) 288.
53 Parihar M S, Ghosh D, Armstrong GA, Yu R, Razavi P & Kranti A, *Appl Phys Lett*, 101 (2012) 093507.
54 Parihar M S &Kranti A, *Nanotechnology*, 26 (2015) 145201.
55 Kumar A, Tripathi M M & Chaujar R, *J Comput Electron*, 17 (2018) 1807.
56 Maiti S, De A & Sarkar S K, *Silicon*, 14 (2022) 6921.
57 Getnet M & Chaujar R, *J Electron Mater*, 51 (2022) 2236.